Research on Measurement Methods for Silicon Carbide Epitaxial Layer Thickness Based on Optical Interference Principles

Siyu Xiong*

School of Science, Jimei University, Xiamen, China, 361021

*Corresponding author: xiongsiyu@jmu.edu.cn

Abstract. As a simple and non-destructive analytical technique, infrared interference spectroscopy is of great value in improving device manufacturing performance due to its ability to accurately measure epitaxial layer thickness. Based on a single-reflection and transmission model, this paper establishes theoretical models for calculating epitaxial layer thickness under two scenarios depending on whether the substrate refractive index is greater or smaller than that of the vacuum. By utilizing the property that substrates with higher carrier concentrations exhibit larger refractive indices, and combining the optical path differences between adjacent beams, an overall interference expression is derived from interference principles. This yields the relationship between fringe order and wavelength, leading to an algorithmic formula for epitaxial layer thickness. Meanwhile, variations in reflectivity are treated as shifts in interference peaks during experiments; adjacent peak values are extracted, corresponding wavenumbers and interference fringe orders are identified, and the thickness is calculated under a given angle of incidence. Under these conditions, two methods are employed to determine the refractive index of the epitaxial layer. In summary, this study provides a theoretical analysis of epitaxial layer thickness and verifies its accuracy through reliability assessments. The proposed methodological framework holds potential for broader application.

Keywords: Silicon Carbide Epitaxial Layers, Dielectric Function, Infrared Spectroscopy, Refractive Index, Optical Interference.

1. Introduction

The substrate is a wafer made of semiconductor single-crystal material, typically with a thickness ranging from 300 μm to 725 μm. The epitaxial layer, on the other hand, is a newly grown single-crystal layer on the processed single-crystal substrate, usually thinner than the substrate. Research on epitaxial layers has already been quite extensive. Chen et al. [1] investigated the process of growing SiC epitaxial layers using chemical vapor deposition on 4° off-axis SiC substrates at different temperatures. They found that higher growth temperatures are beneficial for obtaining epitaxial layers with smooth surfaces and a higher content of 4H-SiC. Yang et al. [2] employed TCS (trichlorosilane) as the silicon source to grow 4H-SiC epitaxial layers within the relatively low temperature range of 1350–1500 °C. The results indicated that a high-quality single-crystal 4H-SiC epitaxial layer could be obtained at 1450 °C. Nozomi Soya et al. [3] reported the observation of an isotropic spin Hall effect in a ferromagnet (epitaxially grown Fe_3Si), which generates a stable spin current with a spin direction that is noncollinear with the magnetization and independent of its orientation. Han et al. [4] systematically modulated the growth temperature to fabricate unipolar epitaxial aluminum nitride films with low oxygen content and high crystalline quality. Their study revealed that films grown at 700 °C exhibited the most favorable overall performance, rendering them suitable for high-performance radio-frequency filter applications. Tang et al. [5] grew 4H-SiC homoepitaxial layers by varying the susceptor rotation speed in a hot-wall CVD reactor, finding that the rotation speed is a key process parameter for increasing the growth rate, improving thickness uniformity, and reducing down-fall defects. Zhao et al. [6] reported a method for preparing semiconducting epitaxial graphene (SEG) on single-crystal silicon carbide substrates via a quasi-equilibrium annealing process. The resulting SEG exhibits a bandgap of 0.6 eV, a room-temperature mobility exceeding 5,000 $cm^2\ V^{-1}\ s^{-1}$, and excellent chemical, mechanical, and thermal stability, making it suitable for nanoelectronic

device applications. Lu et al. [7] investigated the influence of process parameters on the growth rate and thickness uniformity of SiC epitaxial layers in a typical 8-inch hot-wall horizontal SiC epitaxial growth system.

However, most existing studies have focused on experimental investigation of process parameters, with relatively few adopting a mathematical modeling approach to establish theoretical models capable of directly determining or predicting epitaxial layer thickness. To address this gap, this study develops a mathematical model based on infrared interferometry. The model is applied to analyze measurement data obtained from an established experimental source https://www.mcm.edu.cn/html_cn/node/03c91a444e62eee81a3740fa97a461a6.html, with the objective of enabling rapid thickness estimation and providing a theoretical framework for process control.

2. Determination of the Epitaxial Layer Thickness Model Based on Single Reflection and Transmission

This study assumes a vacuum external environment, disregarding variations in factors such as temperature and atmospheric pressure. It is also assumed that both the epitaxial layer and the substrate surface are smooth with uniform thickness. As shown in Figure 1 (a), let the angle of incidence be α, the angle of refraction be β, and the thickness of the epitaxial layer be h. A plane perpendicular to reflected ray 1 is drawn through point B, which serves as the equiphase surface for reflected rays 1 and 2. This equiphase surface intersects reflected ray 1 at point C.

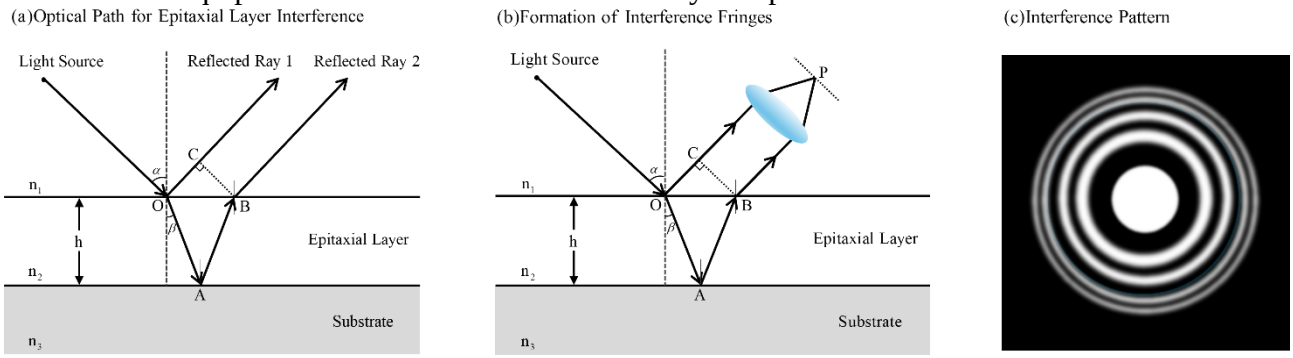

Figure 1 Schematic Diagram of Epitaxial Layer Thickness Measurement

The interference pattern observed is of the equal-inclination type. As illustrated in Figure 1 (b), when incident light strikes the surface, the two reflected rays from the upper and lower interfaces converge via a lens. Varying the angle of incidence produces alternating bright and dark concentric rings, which appear denser toward the outer edges and sparser near the center, as shown in Figure 1 (c).

Numerous experimental studies have shown that when light travels from an optically rarer medium with a lower refractive index to an optically denser medium with a higher refractive index, the reflected wave undergoes a phase shift of π relative to the incident wave—a phenomenon known as "half-wave loss" [8]. It is well established that the refractive index n_2 of the semiconductor material silicon carbide generally falls within the range of approximately 2.0 to 3.5, which is greater than the refractive index of vacuum $n_1 = 1$, i.e., $n_1 < n_2$. Thus, a half-wave loss occurs at this interface. However, the refractive index n_3 of the epitaxial layer is not constant, and its magnitude relative to the substrate refractive index remains undetermined. Therefore, the following discussion will examine the possible cases regarding the magnitude of n_3.

2.1. Problem Solving under the Condition $n_1 < n_2 > n_3$

At the reflection point O of reflected ray 1, light travels from an optically rarer medium to the interface of an optically denser medium, resulting in a half-wave loss for reflected ray 1. Without yet considering the half-wave loss between the epitaxial layer and the substrate, the optical path difference between reflected ray 1 and reflected ray 2 is

$$d_1 = (OA + AB) \cdot n_2 - OC \cdot n_1 \tag{1}$$

Further analysis indicates that since reflected ray 2 undergoes reflection at point A, where light travels from an optically denser medium to the interface of an optically rarer medium, no half-wave loss occurs for ray 2. In summary, the total half-wave loss in the entire process amounts to $\frac{\lambda}{2}$. Therefore, the total optical path difference d is:

$$d = (OA + AB) \cdot n_2 - OC \cdot n_1 + \frac{\lambda}{2} \tag{2}$$

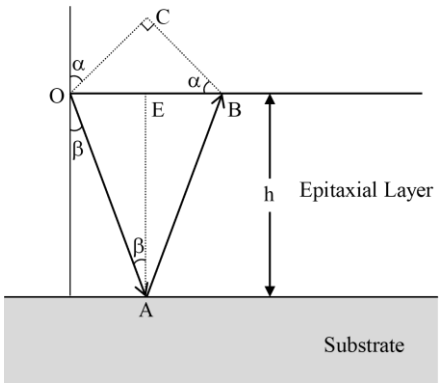

Figure 2 Geometric Optics Schematic for Epitaxial Layer Thickness Measurement

A perpendicular line is drawn through point A intersecting segment OB at point E, as shown in Figure 2. According to the law of reflection, the angle of reflection is α. Thus, $\angle COB = 90^o - \alpha$ and $\angle CBO = \alpha$, leading to $OC = OB \cdot \sin\alpha$. From geometric relations, it can be readily derived that $\angle AOE = \beta$. Since reflection occurs at point A on the substrate, we have $\angle OAE = \angle EAB = \beta$. Given that $OE = h \cdot \tan\beta$, it follows that $OB = 2h \cdot \tan\beta$. Combining the geometric relationships, we obtain $OA = AB = \frac{h}{\cos\beta}$, Hence:

$$OA + AB = \frac{h}{\cos\beta} \tag{3}$$

$$OC = 2h \cdot \sin\alpha \tan\beta \tag{4}$$

Therefore, based on the relative refractive index formula and the principles of optical interference, it is known that when the optical path difference is an integer multiple of the wavelength, the wave crests and troughs of the two beams align constructively, resulting in enhanced interference and the formation of a bright fringe:

$$d = 2h\sqrt{n_2^2 - n_1^2 \sin^2\alpha} + \frac{\lambda}{2} = k\lambda \quad k = 1, 2, L \ , n \tag{5}$$

Conversely, when the optical path difference is an odd multiple of half the wavelength, the crest of one wave aligns with the trough of the other, leading to destructive interference and the formation

of a dark fringe. Similarly, the thickness of the epitaxial layer can be determined under this condition. In summary, when the refractive indices of vacuum, the epitaxial layer, and the substrate satisfy the relation $n_1 < n_2 > n_3$, the corresponding expression is:

$$h = \begin{cases} \dfrac{(2k-1)\lambda}{4\sqrt{n_2^2 - \sin^2\alpha}} & k = 1,2,L\ ,n \\ \dfrac{k\lambda}{2\sqrt{n_2^2 - \sin^2\alpha}} & k = 0,1,L\ ,n \end{cases} \tag{6}$$

2.2. Problem Solving under the Condition $n_1 < n_2 < n_3$

In the case where $n_1 < n_2 < n_3$, at reflection point O of reflected ray 1, light travels from an optically rarer medium to the interface of an optically denser medium, resulting in a half-wave loss for reflected ray 1. Meanwhile, reflected ray 2 undergoes reflection at point A, where light also propagates from an optically rarer medium to an optically denser medium, thus incurring a half-wave loss for ray 2 as well. In summary, although both reflected rays individually experience a half-wave loss, the total effect on the interference pattern is equivalent to the case where no half-wave loss occurs in either reflection, as the half-wave losses occur an even number of times. Therefore, the optical path difference d is:

$$d = 2h\sqrt{n_2^2 - n_1^2\sin^2\alpha} \tag{7}$$

Similarly, it can be concluded that when the relationship between the refractive indices of vacuum, epitaxial layer, and substrate satisfies $n_1 < n_2 < n_3$, the epitaxial thickness h is given by:

$$h = \begin{cases} \dfrac{k\lambda}{2\sqrt{n_2^2 - \sin^2\alpha}} & k = 1,2,L\ ,n \\ \dfrac{(2k-1)\lambda}{4\sqrt{n_2^2 - \sin^2\alpha}} & k = 0,1,L\ ,n \end{cases} \tag{8}$$

3. Derivation of the Epitaxial Thickness Calculation Algorithm

3.1. Method 1

Interference generation requires that the epitaxial layer has a low carrier concentration while the substrate exhibits a high carrier concentration, enabling incident light to reflect at both the surface of the epitaxial layer and the interface between the epitaxial layer and the substrate. According to the free-carrier effect, a higher carrier concentration leads to a lower refractive index [9], i.e., $n_2 > n_3$. Therefore, the optical path difference is given by:

$$d = 2h\sqrt{n_2^2 - n_1^2\sin^2\alpha} + \frac{\lambda}{2} \tag{9}$$

Furthermore, the equations for maximum and minimum interference can be derived from constructive and destructive interference, respectively, as follows:

$$2h\sqrt{n_2^2 - n_1^2\sin^2\alpha} = m\lambda_m \tag{10}$$

Here, m represents the fringe order at wavelength λ_m. If m is an integer, it corresponds to a minimum in interference; if m is an odd half-integer (i.e., an odd multiple of $\frac{1}{2}$, it corresponds to a maximum. Generally, the product $m\lambda_m$ remains constant, i.e.,

$$m\lambda_m = (m+x)\lambda_{m+x} = C \tag{11}$$

thus m can be solved as:

$$m = \frac{X \cdot \lambda_{m+x}}{\lambda_m - \lambda_{m+x}} \tag{12}$$

where the integer x denotes the number of fringes between the wavelengths λ_m and λ_{m+x}.

Under equilibrium conditions, this quantity remains constant. Therefore, this study primarily investigates the relationship between the wavelength λ and the refractive index n_2 of the epitaxial layer.By reviewing relevant literature [10], this work draws on the application of the minimum deviation angle method reported in prior research, leading to an expression that describes the variation of refractive index with wavelength.

$$n_2^2 - 1 = \frac{5.5394\lambda^2}{\lambda^2 - 0.026945} \tag{13}$$

Through experimental validation in published research, the refractive index n3*n*3 of silicon carbide (SiC) was determined to be 2.6473. By rearranging the aforementioned formula, the thickness of the epitaxial layer can be expressed as:

$$h = \frac{m\lambda_m}{2\sqrt{n_2^2 - n_1^2 \sin^2\alpha}} \tag{14}$$

By substituting the refractive index of vacuum $n_1 = 1$ and combining it with the formula from the literature, the average refractive index of the epitaxial layer $n_2 = 3.8769$ is obtained. Accordingly, the expression for h can be derived as:

$$h = \frac{m\lambda_m}{2\sqrt{3.8769^2 - \sin^2\alpha}} \tag{15}$$

Next, in this paper, the test result data of the silicon carbide wafer (with incident angles of 10° and 15° respectively) retrieved from the URL are plotted as graphs. It can be observed that the curves exhibit multiple peaks. In this study, we use code to identify the peaks in each region and extract the wavenumbers corresponding to these peaks. The peak detection process is illustrated in Figures 3 and 4.

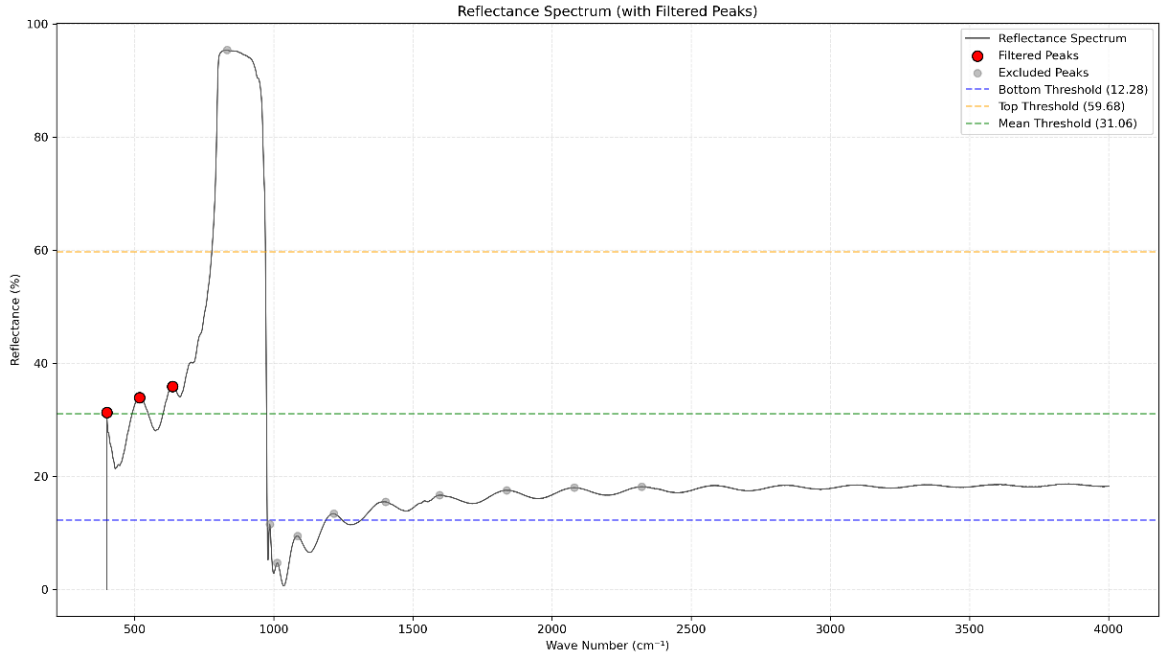

Figure 3 Reflectance Spectrum at 10°Incident Angle

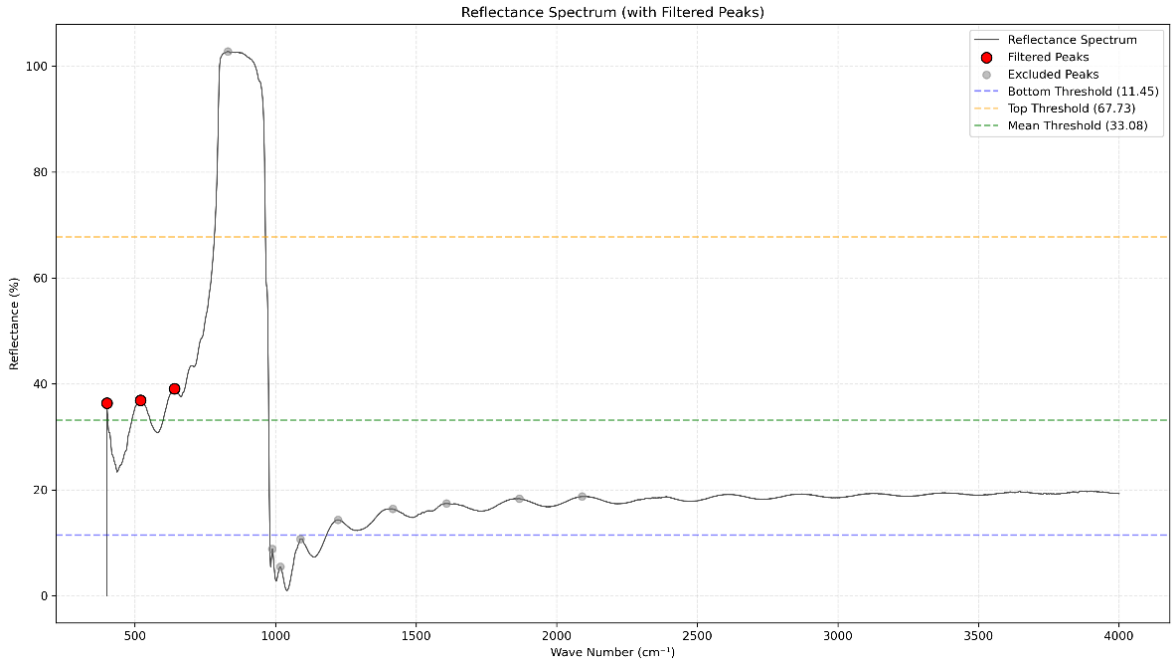

Figure 4 Reflectance Spectrum at 15°Incident Angle

Next, the corresponding wavelength is calculated using $\lambda = \frac{1}{\nu}$. Then, the formula $m = \frac{x\lambda_{m+x}}{\lambda_m - \lambda_{m+x}}$ is applied to the wavelengths corresponding to adjacent wave peaks. Specifically, when $x = 1$, the fringe number m for local maximum interference can be obtained by computing the wavenumber values corresponding to adjacent wave peaks in the graph. Finally, $m\lambda_m$ is derived.

Finally, the average epitaxial layer thicknesses of $10.92\,\mu m$ and $10.79\,\mu m$ can be derived from the experimental result data. However, it is readily apparent that this method has a limitation: due to the relatively subjective selection of peak points, the final results obtained will vary. Therefore, we further propose a second method (Method 2) to address this issue.

3.2. Method 2

Considering the variable refractive index of silicon carbide (SiC) epitaxial layers due to carrier doping, this study comprehensively accounts for the influence of carrier concentration and incident light wavelength on the refractive index of the epitaxial layer. Based on the principle of determining quality parameters via infrared reflection spectra [11], an expression for the refractive index is derived. To control variables and address the fact that different grain orientations lead to different refractive indices, the most common $4H-SiC$ polar uniaxial crystal is selected as the subject of this investigation.

3.2.1 Dielectric Function

According to the literature, when the carrier concentration is below $10^{16}cm^{-3}$ and the carrier concentration of $4H-SiC$ is $5.2\times10^{15}cm^{-3}$, the plasma frequency and plasma damping constant are relatively small. Compared to lattice vibrations, the contribution of plasma infrared response formed by carriers can be neglected. Therefore, the formula for the infrared dielectric function can be simplified as:

$$\varepsilon(\nu)=\varepsilon_{0}\frac{(\nu^{2}-\nu_{L}^{2}+j\gamma_{L}\nu)}{(\nu^{2}-\nu_{T}^{2}+j\gamma_{T}\nu)} \tag{16}$$

Here, ν denotes the wavenumber of infrared light, and ε_0 is the high-frequency dielectric constant, which refers to the dielectric constant of the material at extremely high optical frequencies. ν_T represents the transverse optical (TO) phonon frequency of the SiC lattice, while ν_L is the longitudinal optical (LO) phonon frequency of the lattice; ν_T and ν_L characterize the intrinsic vibrational properties of the SiC crystal. γ_T and γ_L are the attenuation constants corresponding to the respective directions. In the expression of the dielectric function, $j\gamma_L\nu$ is typically used to describe energy loss or attenuation.

Based on the relationship between the dielectric function and the complex refractive index, given by $\varepsilon=\varepsilon_{r}(\nu)+j\varepsilon_{i}(\nu)=(n(\nu)+jk(\nu))^{2}$, we can derive the real and imaginary parts of the infrared-responsive dielectric function of silicon carbide (SiC) as follows:

$$\varepsilon_{r}(\nu)=n^{2}(\nu)-k^{2}(\nu)=\varepsilon_{0}\frac{\left[(\nu^{2}-\nu_{T}^{2})(\nu^{2}-\nu_{L}^{2})+\gamma_{T}\gamma_{L}\nu^{2}\right]}{(\nu^{2}-\nu_{T}^{2})^{2}+(\gamma_{T}\nu)^{2}} \tag{17}$$

$$\varepsilon_{i}(\nu)=2n(\nu)k(\nu)=\varepsilon_{0}\frac{\left[\gamma_{T}\nu(\nu^{2}-\nu_{T}^{2})-\gamma_{L}\nu(\nu^{2}-\nu_{L}^{2})\right]}{(\nu^{2}-\nu_{T}^{2})^{2}+(\gamma_{T}\nu)^{2}} \tag{18}$$

Meanwhile, it can be concluded that the maximum of $\frac{dR}{d\nu}$ occurs at the peak of $\varepsilon_i(\nu)$, i.e., at ν_T; conversely, another maximum of $\frac{dR}{d\nu}$ corresponds to the peak of the imaginary part of the energy-loss function $(\frac{-1}{\varepsilon(\nu)})_i$, i.e., at ν_L. Based on this, we can differentiate the data points from the reflectance spectrum obtained via experimental data. By identifying the wavenumbers corresponding to the highest or lowest slopes at individual points, ν_T and ν_L can thus be determined.

3.2.2 Grain Orientation Theorem

Owing to the anisotropy of crystals, the transverse optical (TO) phonon frequency ν_T of the SiC lattice can be expressed as ν_{AT} and ν_{ET}, where the subscripts A and E denote atomic

displacements parallel and perpendicular to the optical axis, respectively. Correspondingly, both the static dielectric constant and the high-frequency dielectric constant can be categorized into components parallel to the optical axis ε_{A1}, ε_{A0} and those perpendicular to the optical axis ε_{E1}, ε_{E0}.In practical research, the electronegativity difference between Si and C atoms gives rise to a macroscopic longitudinal electrostatic field (when the two atoms undergo relative motion) — a field that induces longitudinal-transverse splitting of the optical modes. As a result, the longitudinal phonon frequency (for displacements in both directions) is higher than the transverse phonon frequency. By incorporating the properties of the 4H-SiC crystal, the parameter values at the Γ-point in the Brillouin zone can be obtained, as detailed in Table 1.

Table 1 Parameters of 4H-SiC at the Γ-point in the Brillouin zone

ν_{AT}/cm^{-1}	ν_{AL}/cm^{-1}	ν_{ET}/cm^{-1}	ν_{EL}/cm^{-1}	$\varepsilon_{A\infty}$(300K)	$\varepsilon_{E\infty}$(300K)
783.6	964.2	796.6	972.7	6.78	6.56

Here, the Γ-point is a special high-symmetry point in the Brillouin zone, typically corresponding to a wave vector of 0. Thus, it can be seen from the table that the high-frequency dielectric constant of the 4H-SiC crystal exhibits anisotropy.The longitudinal and transverse optical phonon frequencies of the mixed phonons can be derived using the Loudon formula, as follows:

$$v_T^{\ 2} = v_{ET}^2 \sin^2\theta + v_{AT}^2 \cos^2\theta \tag{19}$$

$$v_L^{\ 2} = v_{EL}^2 \sin^2\theta + v_{AL}^2 \cos^2\theta \tag{20}$$

By substituting ν_T and ν_L (determined from the experimental data) into the relevant formula, the angle θ between the incident light and the crystal's optical axis can be obtained, thereby determining the grain orientation.

On the basis of the obtained angle θ, we can derive ε_0 using the relational expression between the high-frequency dielectric constant and the angle with the optical axis:

$$\varepsilon_0 = \frac{\varepsilon_{A0}\varepsilon_{E0}}{\varepsilon_{A0}\cos^2\theta + \varepsilon_{E0}\sin^2\theta} \tag{21}$$

The refractive index corresponds to the real part of the complex refractive index; thus, the refractive index of the epitaxial layer can be obtained using the above relational expression:

$$n_2 = \left[\frac{\sqrt{\varepsilon_r^{\ 2} + \varepsilon_i^{\ 2}} + \varepsilon_r}{2}\right]^{\frac{1}{2}} \tag{22}$$

The expression for the extinction coefficient is given by:

$$k = \left[\frac{\sqrt{\varepsilon_r^{\ 2} + \varepsilon_i^{\ 2}} - \varepsilon_r}{2}\right]^{\frac{1}{2}} \tag{23}$$

For the energy loss caused by absorption in the epitaxial layer, this paper investigates the influence of different parameters on the loss through modeling. Using the least squares estimation method, we obtain the optimally matched attenuation constants γ_T and γ_L at different wavenumbers, and then derive the refractive index of the epitaxial layer corresponding to these wavenumbers.

The formula for the dielectric function is given by:

$$\varepsilon(\nu) = \varepsilon_0 \left[\frac{(\nu^2 - \nu_L^2 + j\gamma_L \nu)}{(\nu^2 - \nu_T^2 + j\gamma_T \nu)} - \frac{\nu_p{}^2}{\nu^2 + j\gamma_p \nu} \right] \tag{24}$$

Here, the term $-\frac{\nu_p{}^2}{\nu^2 + j\gamma_p \nu}$ is the Drude term (also referred to as the free carrier term), which accounts for the contribution of charge carriers. ν_p denotes the plasma frequency, and λ_p is the plasma damping constant. The dielectric function at the plasma frequency is dominated by the phonon frequency, and there exists a loss induced by the absorption of the epitaxial layer medium. This loss effect is represented by γ_T and γ_L, which are also called damping coefficients. This paper focuses on the influence of wavenumber on the loss constant; thus, the expression for the frequency dependence of the damping coefficient (on light frequency) can be approximately derived as follows:

$$\gamma(\nu) = \gamma_0 + A\nu + B\nu^2 + C\nu^3 + D\nu^4 \tag{25}$$

Based on the damping coefficients, the phonon lifetime can be derived:

$$t = \frac{1}{2\pi c\gamma} \tag{26}$$

Here, c denotes the speed of light. This formula describes the decay rate of lattice vibrations, reflecting the dependence of the decay rate on the optical frequency.

Next, from the relationship between the dielectric function and the complex refractive index, $\varepsilon = \varepsilon_r(\nu) + j\varepsilon_i(\nu) = (n(\nu) + jk(\nu))^2$, the expression for the complex refractive index can be obtained as follows:

$$\bar{n}(\nu) = n(\nu) + jk(\nu) = \sqrt{\varepsilon(\nu)} \tag{27}$$

By incorporating Fresnel's theorem, the known reflectance data in the attachment can be used to solve for the complex refractive index. Considering that the incident light is obliquely incident, the reflection coefficient formulas can be derived as follows:

For s-polarized light:

$$r_s(\nu) = \frac{\cos\alpha - \bar{n}(\nu)\cos\beta}{\cos\alpha + \bar{n}(\nu)\cos\beta} \tag{28}$$

For p-polarized light:

$$r_p(\nu) = \frac{\bar{n}(\nu)\cos\alpha - \cos\beta}{\bar{n}(\nu)\cos\alpha + \cos\beta} \tag{29}$$

Assuming that the two polarization states are mixed with equal probability, the expression for the total reflectance is obtained as:

$$R_{total} = \frac{R_s(\nu) + R_p(\nu)}{2} = \frac{|r_s(\nu)|^2 + |r_p(\nu)|^2}{2} \tag{30}$$

This allows us to link the reflectance, wavenumber, and dielectric function, yielding the parameters to be fitted. These parameters include the coefficients in the expressions describing how the transverse and longitudinal damping coefficients depend on the optical frequency. They also include ν_T and ν_L, which correspond to the positions of the maximum and minimum derivatives

in the reflectance spectrum. Additionally, the parameters to be fitted include two parameters: ν_P and λ_P.

We apply the formulas derived in this section to the data for calculation. Through fitting via the nonlinear least-squares method, we finally determine the loss degree of charge carriers on interference propagation and the refractive index of the epitaxial layer under multiple sets of wavenumber and reflectance conditions.

Through code execution and calculation, we can obtain ν_T, ν_L, the angle θ between the incident light and the crystal's optical axis, and the high-frequency dielectric constant ε_0. The specific results are presented in Table 2 below:

Table 2 The parameter results related to the dielectric function

Data	ν_T	ν_L	θ	ε_0
$\alpha = 10^o$	796.0 cm^{-1}	973.4 cm^{-1}	77.28°	6.769
$\alpha = 15^o$	796.0 cm^{-1}	975.8 cm^{-1}	77.28°	6.769

Subsequently, the data from the table were substituted into the equations, yielding the values of relevant parameters at different wave numbers. Due to space limitations, only a subset of the data is presented here, as shown in Table 3.

Table 3 Optical interference parameter table vs. frequency

Wave Number	TO phonon damping	LO Phonon Damping	Re(ε)	Im(ε)	TO Phonon Lifetime	LO Phonon Lifetime	Refrac-tive Index	Extinction Coefficient
399.675	38.898	39.898	10.976	0.134	0.136	0.133	3.313	0.020
403.279	40.038	41.038	11.002	0.141	0.133	0.129	3.317	0.021
406.883	41.207	42.207	11.028	0.149	0.129	0.126	3.321	0.022
410.487	42.404	43.404	11.055	0.157	0.125	0.122	3.325	0.024
414.091	43.632	44.632	11.082	0.165	0.122	0.119	3.329	0.025
417.695	44.889	45.889	11.110	0.173	0.118	0.116	3.333	0.026
421.299	46.178	47.178	11.139	0.182	0.115	0.113	3.338	0.027
424.903	47.497	48.497	11.168	0.192	0.112	0.109	3.342	0.029
428.507	48.849	49.849	11.197	0.202	0.109	0.106	3.346	0.030
432.111	50.232	51.232	11.227	0.213	0.106	0.104	3.351	0.032

From this, the variation of parameters at different optical frequencies can be determined, yielding the corresponding values of the refractive index. Subsequently, by combining the epitaxial layer thickness formula $h = \frac{m\lambda_m}{2\sqrt{n_2^2 - \sin^2\alpha}}$ with the reflectance spectrum, suitable local peaks are identified. The wavenumbers corresponding to these peaks are extracted, and the epitaxial layer thickness is calculated at each corresponding wavenumber. Finally, the thickness values are averaged to obtain the thickness estimates, which are 7.966 μm and 13.671 μm, respectively.

4. Conclusions

This paper begins by establishing mathematical models for determining the thickness of the epitaxial layer from the perspective of geometric optics, considering two distinct scenarios. Furthermore, it investigates two methods for measuring the thickness of silicon carbide epitaxial layers based on infrared reflectance spectroscopy. Method 1 primarily relies on interference fringe analysis but suffers from subjectivity, whereas Method 2 employs a more sophisticated dielectric function model to achieve more accurate retrieval of epitaxial layer parameters, making it the superior choice for high-quality process control.

References

[1] Chen J, Guan M, Yang S, et al. Characterization of epitaxial layers grown on 4H-SiC (0 0 0− 1) substrates[J]. Journal of Crystal Growth, 2023, 604: 127048.

[2] Yang S, Zhao S, Chen J, et al. Growth of 4H-SiC epitaxial layers at temperatures below 1500 C using trichlorosilane (TCS)[J]. Journal of Crystal Growth, 2023, 612: 127058.

[3] Soya N, Yamada M, Hamaya K, et al. Isotropic spin Hall effect in an epitaxial ferromagnet[J]. Physical review letters, 2023, 131(7): 076702.

[4] Han C, **ao X, Zhang W, et al. Impact and role of epitaxial growth in metal halide perovskite solar cells[J]. ACS Materials Letters, 2023, 5(9): 2445-2463.

[5] Tang Z, Gu L, ** L, et al. Insights into the effect of susceptor rotational speed in CVD reactor on the quality of 4H-SiC epitaxial layer on homogeneous substrates[J]. Materials Today Communications, 2024, 38: 108037.

[6] Zhao Zhi, Ji P., Li Yi, et al. Ultrahigh-mobility semiconducting epitaxial graphene on silicon carbide [J]. *Nature*, 2024, 625(7993): 60-65.

[7] Lu Runlin, Zheng Lili, Zhang Hui, et al. Effect of hot-wall CVD process parameters on thickness uniformity of 8-inch SiC epitaxial layers[J]. Journal of Synthetic Crystals, 2025, 54(9).

[8] Zhang Honggen. On the Teaching Articulation of "Half-wave Loss" Between University and Middle School Physics[J]. Friends of Physics, 2022, 38(02): 47-49+52.

[9] Chen Kejian, Yang Ailing, Jiang Xiaoqing. Modeling of Photogenerated Carrier Effects on Refractive Index in Semiconductor Waveguide Materials[J]. Optical Instruments, 2002 (5): 34-38.

[10] Fischer M P, Bühler J, Fitzky G, et al. Coherent field transients below 15 THz from phase-matched difference frequency generation in 4H-SiC[J]. Optics letters, 2017, 42(14): 2687-2690.

[11] Ma Gelin, Zhang Yuming, Zhang Yimen, et al. Novel evaluation technique for quality of silicon carbide epitaxial layers[J]. Journal of Xidian University, 2011, 38(6): 37-43.

[1]